Narges Kaynia
Department of Mechanical Engineering,
Massachusetts Institute of Technology,
Cambridge, MA 02139
e-mail: nkaynia@mit.edu

Elaine Soohoo
Departments of Mechanical Engineering and Bioengineering,
University of California,
Berkeley, CA 94720
e-mail: soohoo.elaine@gmail.com

Tony M. Keaveny
Departments of Mechanical Engineering and Bioengineering,
University of California,
Berkeley, CA 94720
e-mail: tmk@me.berkeley.edu

Galateia J. Kazakia[1]
Department of Radiology and Biomedical Imaging,
University of California San Francisco,
185 Berry Street, Suite 350,
San Francisco, CA 94107
e-mail: galateia.kazakia@ucsf.edu

Effect of Intraspecimen Spatial Variation in Tissue Mineral Density on the Apparent Stiffness of Trabecular Bone

This study investigated the effects of intraspecimen variations in tissue mineral density (TMD) on the apparent-level stiffness of human trabecular bone. High-resolution finite element (FE) models were created for each of 12 human trabecular bone specimens, using both microcomputed tomography (μCT) and "gold-standard" synchrotron radiation μCT (SRμCT) data. Our results confirm that incorporating TMD spatial variation reduces the calculated apparent stiffness compared to homogeneous TMD models. This effect exists for both μCT- and SRμCT-based FE models, but is exaggerated in μCT-based models. This study provides a direct comparison of μCT to SRμCT data and is thereby able to conclude that the influence of including TMD heterogeneity is overestimated in μCT-based models. [DOI: 10.1115/1.4029178]

Keywords: trabecular bone, tissue mineral density, heterogeneity, finite element analysis, microcomputed tomography, synchrotron, mechanical properties, apparent modulus

Introduction

The mechanical behavior of human trabecular bone plays an important role in the load-bearing function of the skeleton and is significantly impacted in common medical conditions such as osteoporosis. The mechanical behavior of trabecular bone is determined by several factors including bone volume fraction (BV/TV), microstructure, and—the main topic of this study—the material properties of the bone tissue. The effect of microstructure on the overall "apparent-level" mechanical behavior of trabecular bone specimens (typically at the scale of 5–10 mm) has been investigated in several computational studies [1–5]. However, these studies typically assume homogeneous material properties for the bone tissue at the "tissue level" (typically at the scale of 100 μm or less), neglecting to account for any spatial variations in the TMD. These variations are the result of normal bone remodeling [6,7], can be altered by osteoporosis treatments [6,8–10], and have been shown to directly influence the mechanical properties of bone tissue [11–17].

Previous studies have attempted to quantify the effect of TMD variation on the mechanical properties of bone tissue. These studies have incorporated spatial variations in TMD by creating heterogeneous high-resolution μCT-based FE models. FE models with applied variations in mineralization based on different algorithms [17,18] as well as FE models where the heterogeneity in the mineralization is measured from high-resolution μCT images of the trabecular bone [11,14–17,19] have been investigated. These studies all demonstrated that a trabecular bone model that accounts for TMD heterogeneity will predict lower apparent stiffness than a model with homogeneous TMD. However, these studies were limited by the resolution and quality of the μCT images and therefore capture only the TMD variations detectable by μCT. In fact, μCT-based TMD measurement is influenced by substantial artifacts resulting from the polychromatic X-ray source and cone-shaped beam [20]. High energy, parallel-beam, monochromatic SRμCT is considered the gold standard in assessing TMD variation in trabecular bone.

Addressing these limitations of conventional μCT imaging, the goal of this study was to evaluate the influence of TMD variation in μCT-based FE models compared to gold standard SRμCT-based FE models. The results derived from this work improve understanding of how spatial variations in tissue material properties can influence apparent level properties and provide insight into the imaging methodologies used to assess the microstructure and micromechanics of trabecular bone.

Materials and Method

Study Design. In this study, μCT- and SRμCT-based FE analyses were performed on 12 human trabecular bone samples, all taken from unique donors. Human trabecular bone from several anatomic sites (femoral head, proximal tibia, and vertebra) was used to enable the interpretation of findings in the context of varying bone structure. The μCT and SRμCT imaging was used to define microstructure and characterize the spatial variation in mineralization, while FE modeling was used to characterize mechanical behavior.

A main feature of this study design is the ability to determine and isolate any biomechanical effects associated with material heterogeneity from those effects associated with microstructure. Further, the effects of intraspecimen TMD variation were isolated from interspecimen TMD variation. To achieve this, we considered three virtually altered mineralization cases for each μCT and SRμCT scan (Fig. 1): (1) a heterogeneous model with spatially varying mineralization throughout the bone as measured directly by μCT or SRμCT; (2) a specimen-specific homogeneous model with the mean TMD value assigned to all bone tissue; and (3) a reference value homogeneous model with a constant reference

[1]Corresponding author.

Manuscript received August 5, 2014; final manuscript received November 17, 2014; accepted manuscript posted December 10, 2014; published online December 10, 2014. Assoc. Editor: Blaine A. Christiansen.

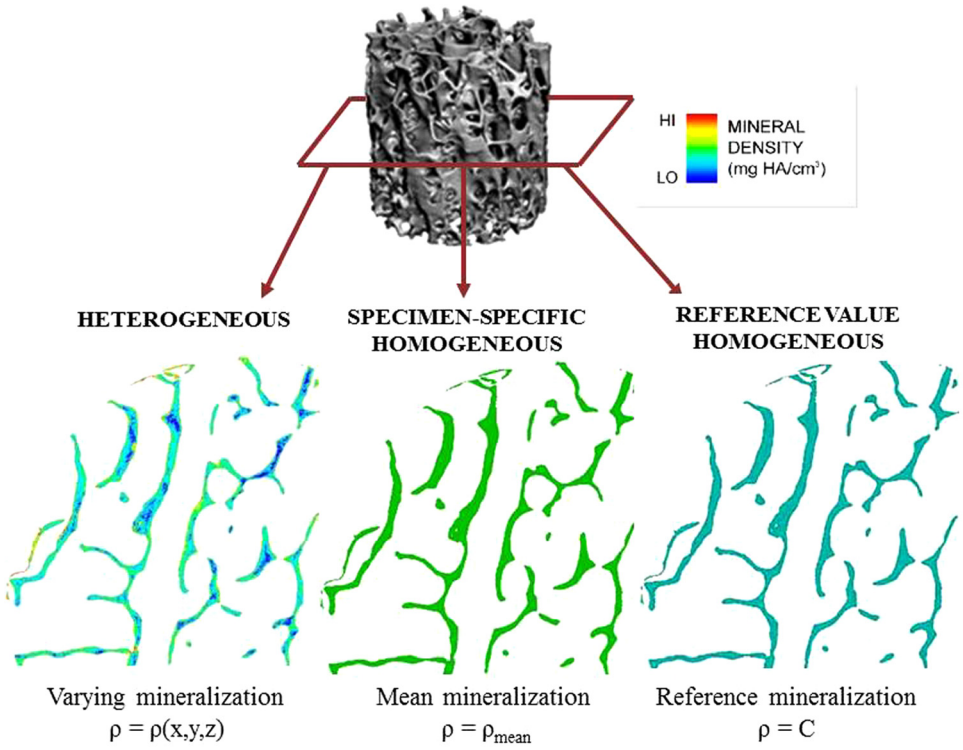

Fig. 1 Schematic representation of the three material models evaluated for each specimen

TMD value for all bone tissue across all specimens. This resulted in three different models to evaluate for each of the 12 human trabecular bone specimens imaged by μCT and SRμCT (a total of 72 simulations and analyses).

Specimen Preparation. UCSF Committee for Human Research approval was granted for this work. Trabecular specimens were isolated from the femoral head (FEM, $n = 4$), vertebral body (VERT, $n = 5$), and proximal tibia (TIB, $n = 3$). Femoral head specimens were surgically excised during hip arthroplasty procedures at UCSF. Vertebrae and tibiae were harvested from human cadavers (National Disease Research Interchange, Philadelphia, PA). Each specimen was obtained from a unique donor. Each cylinder of trabecular bone (8 mm diameter and 4 mm length) was machined with the axis aligned in the superior–inferior orientation. The specimens were cleaned of marrow using a water jet with sonicator agitation and detergent washes as necessary (1%, Tergazyme, Alconox, Inc.). The specimens were stored at −20 °C when not being processed.

***μ*CT Scanning.** The trabecular bone specimens were scanned using a μCT scanner (μCT-40 Scanco Medical AG., Bruttisellen, Switzerland). Imaging was performed at an isotropic voxel size of 8 μm using 70 kV source potential and 114 μA tube current. Each scan consisted of 2000 projections over 360 deg, with a 250 ms integration time per projection. Scan time was 11–12 h per specimen. Three-dimensional data sets were reconstructed using a cone beam approximation [21]. Attenuation values were converted to hydroxyapatite (HA) density in units of mgHA/cm^3 using a HA calibration phantom and a beam hardening correction algorithm. Details of the calibration process and correction have been reported previously [20,22].

SR*μ*CT Scanning. SRμCT imaging was performed on beamline X2B of the National Synchrotron Light Source (Brookhaven National Laboratory, Upton, NY). This beamline is equipped with a monochromator to create a specific narrow energy incident beam. All specimens were scanned under identical conditions using a 26 keV beam selected based on an established energy optimization protocol that produces less than 0.1% variations in linear attenuation [20,23]. Each scan consisted of 1440 projections over 360 deg, with an integration time of 1800–2200 ms per projection. Typical scan time was 3–4 h per specimen. A filtered back-projection algorithm was applied to reconstruct three-dimensional images with isotropic voxel size of 7.5 μm, which were subsequently rescaled to isotropic 8 μm voxels. The same HA-calibration phantom used for the μCT images was scanned under the same conditions as the bone specimens and used to convert SRμCT attenuation values to mgHA/cm^3. A comparison of image quality and density histograms is included in a previous publication [20].

FE Modeling. The reconstructed three-dimensional μCT and SRμCT data sets were masked to isolate bone from background using a manual thresholding scheme (IPL v5.01 c-ucsf, Scanco Medical AG). A single threshold value was determined for each anatomic site, based on the best delineation of bone surfaces and voids when visually compared to the original images. Thresholds were determined independently for μCT (FEM = 576 mgHA/cm^3; TIB and VERT = 556 mgHA/cm^3) and SRμCT (FEM = 715 mgHA/cm^3, TIB and VERT = 556 mgHA/cm^3). A comparison to alternate, automated thresholding schemes is described in a previous publication [20].

Using the binarized μCT and SRμCT images, BV/TV was computed by direct voxel counting [24]. Masked μCT and SRμCT images were used to calculate mean TMD. In this process, the outer two voxel layers were temporarily eroded from the bone surfaces (IDL v6.2, ITT) to minimize any effects of partial volume averaging [25].

FE models were constructed and analyzed using custom in-house software built on a highly scalable, implicit parallel FE framework [26]. Three-dimensional FE models were created by constructing an eight-noded hexahedral brick element with the side dimensions of 8 μm for every voxel in each μCT and SRμCT volume. The fine mesh used in this study ensures that the most important features of the trabecular bone and the mineral

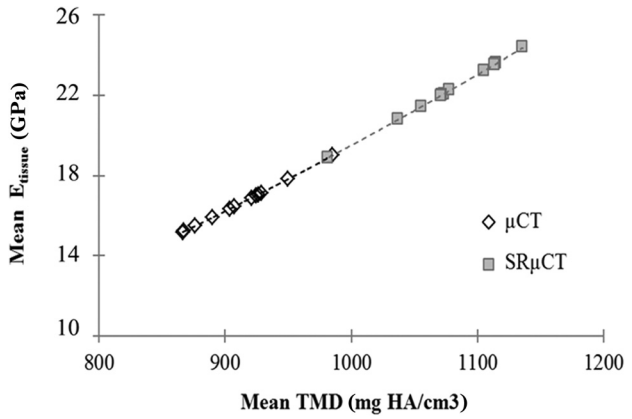

Fig. 2 Mean E_{tissue} plotted against mean TMD for each specimen as calculated from μCT and SRμCT images ($n = 12$)

distribution were captured properly [27]. The FE models contained 14×10^6–139×10^6 elements and 48 million to 456 million degrees of freedom.

High-resolution, linearly elastic, FE analysis was used to simulate a uniform compression test under 1% uniaxial compressive strain. A power-law was used to assign a tissue modulus (E_{tissue}) to each element in the models based on the element's mineral density. The relationship used in this study was established by Easley et al. [19], by evaluating a compilation of data from the literature [19,28–30]

$$E_{tissue} = (1.127 \times 10^{-4}) \times \mathrm{TMD}^{1.746} \quad (1)$$

where unit of E_{tissue} is GPa and unit of TMD is mgHA/cm^3.

Three models were evaluated for each μCT and SRμCT data set (Fig. 1). In the heterogeneous model, we deployed the voxel-specific TMD directly obtained from the scan to assign a unique E_{tissue} (using Eq. (1)) to each element in the FE model, to then calculate the apparent heterogeneous modulus (E^{HET}). This stiffness measure includes effects of TMD variations within and across specimens as well as microstructure variations across specimens. In the specimen-specific homogeneous model, we applied the specimen-specific mean TMD to assign a single mean E_{tissue} (Fig. 2) uniformly to all elements in the model, to then calculate the apparent specimen-specific homogeneous modulus (E^{HOM}). This stiffness measure includes effects of the interspecimen variation in mean TMD as well as variations in microstructure, but does not include the effects of intraspecimen spatial TMD variations. In the reference value homogeneous model, we applied a constant reference E_{tissue} uniformly to all elements in all models to calculate the apparent reference value homogeneous modulus (E^{REF}). The reference E_{tissue} value (19,395 MPa) is the average of all specimen-specific mean E_{tissue} values calculated for all μCT and SRμCT data sets. E^{REF} is influenced solely by bone microstructure and does not include effects of inter- or intraspecimen TMD variation. In each case, apparent modulus was calculated as the ratio of the apparent stress (total reaction force divided by total cross section area) to the applied strain.

A series of normalized stiffness measures were calculated to consider the individual contributions of TMD variations and microstructural differences to the FE analysis results. To examine the influence of intra- and interspecimen TMD variation (excluding the effects of microstructure), normalized stiffness E^{HET}/E^{REF} was computed. To isolate interspecimen TMD variation, normalized stiffness E^{HOM}/E^{REF} was computed. To isolate the influence of intraspecimen TMD variation, normalized stiffness E^{HET}/E^{HOM} was computed.

Statistical Analysis. Summary statistics were compiled using mean and standard deviation calculations. Because of the small sample sizes, some outcome parameter distributions were not normally distributed and thus nonparametric statistics were used. Paired Wilcoxon Signed Rank tests and general linear regression were used to compare μCT and SRμCT outcome measures. Bland–Altman analyses were also performed to assess the agreement between μCT and SRμCT results. For analyses comparing apparent modulus values, specimens were separated into low BV/TV ($\leq$0.20) and high BV/TV (>0.20) groups. The low BV/TV group included all TIB and VERT specimens, while the high BV/TV group included all FEM specimens (Table 1). For all tests, $p < 0.05$ was considered statistically significant. JMP (version 10, SAS) and Excel (2010, Microsoft) were used for statistical analysis.

Results

Apparent stiffness calculated from the μCT and SRμCT FE models correlated well; however, μCT-based FE analysis underestimated apparent modulus in both homogeneous and heterogeneous specimen-specific models. Linear regression between μCT and SRμCT values of E^{HET}, E^{HOM}, and E^{REF} produced correlations with $R^2 > 0.99$ (Fig. 3). Bland–Altman analysis revealed that μCT-based E^{HET} and E^{HOM} were underestimated by 26% and 22%, respectively, compared to SRμCT-based values. In contrast, μCT-based E^{REF} was overestimated by only 4%, reflecting the accuracy of microstructure determination by μCT. Paired Wilcoxon Signed Rank tests detected significant differences between μCT and SRμCT values for the entire range of BV/TV ($p = 0.0005$ E^{HET} and E^{HOM} and $p = 0.003$ E^{REF})

Including intraspecimen TMD heterogeneity reduced the apparent stiffness calculated from both the μCT and SRμCT FE models. The calculated apparent modulus was lower in heterogeneous models compared to specimen-specific homogeneous models ($E^{HET} < E^{HOM}$; $p = 0.0005$). This outcome was consistent for low and high BV/TV samples and for models created from both the μCT and SRμCT images (Fig. 4). In the low BV/TV group, E^{HET} was lower than E^{HOM} by 15% (48 MPa) and 12% (47 MPa) for μCT and SRμCT, respectively (each $p = 0.008$). In the high BV/TV group, E^{HET} was lower by 14% (222 MPa) and 9% (194 MPa) for μCT and SRμCT, respectively (each $p = 0.125$).

With the influence of specimen microstructure eliminated, including TMD heterogeneity again reduced the apparent stiffness calculated from both the μCT and SRμCT FE models. In order to remove the influence of microstructure and thereby isolate the influence of intra- and interspecimen TMD variations, E^{HET}/E^{REF} and E^{HOM}/E^{REF} were calculated for the μCT and SRμCT models (Fig. 5). Normalization with E^{REF} eliminated the distinction between low and high BV/TV groups; therefore, all specimens were considered together. Mean differences between the normalized values E^{HET}/E^{REF} and E^{HOM}/E^{REF} were 18% (0.13 MPa/

Table 1 Donor and specimen information grouped by anatomic site

	Age (mean ± SD, range)	Sex (M/F)	μCT BV/TV (mean ± SD, range)	SRμCT BV/TV (mean ± SD, range)
Femoral head	63 ± 9, 50–71	2/2	0.33 ± 0.04, 0.29–0.37	0.32 ± 0.03, 0.28–0.36
Vertebra	70 ± 3, 66–76	4/1	0.09 ± 0.03, 0.06–0.13	0.09 ± 0.03, 0.06–0.12
Proximal tibia	58 ± 9, 50–70	2/1	0.08 ± 0.02, 0.05–0.10	0.07 ± 0.02, 0.05–0.10

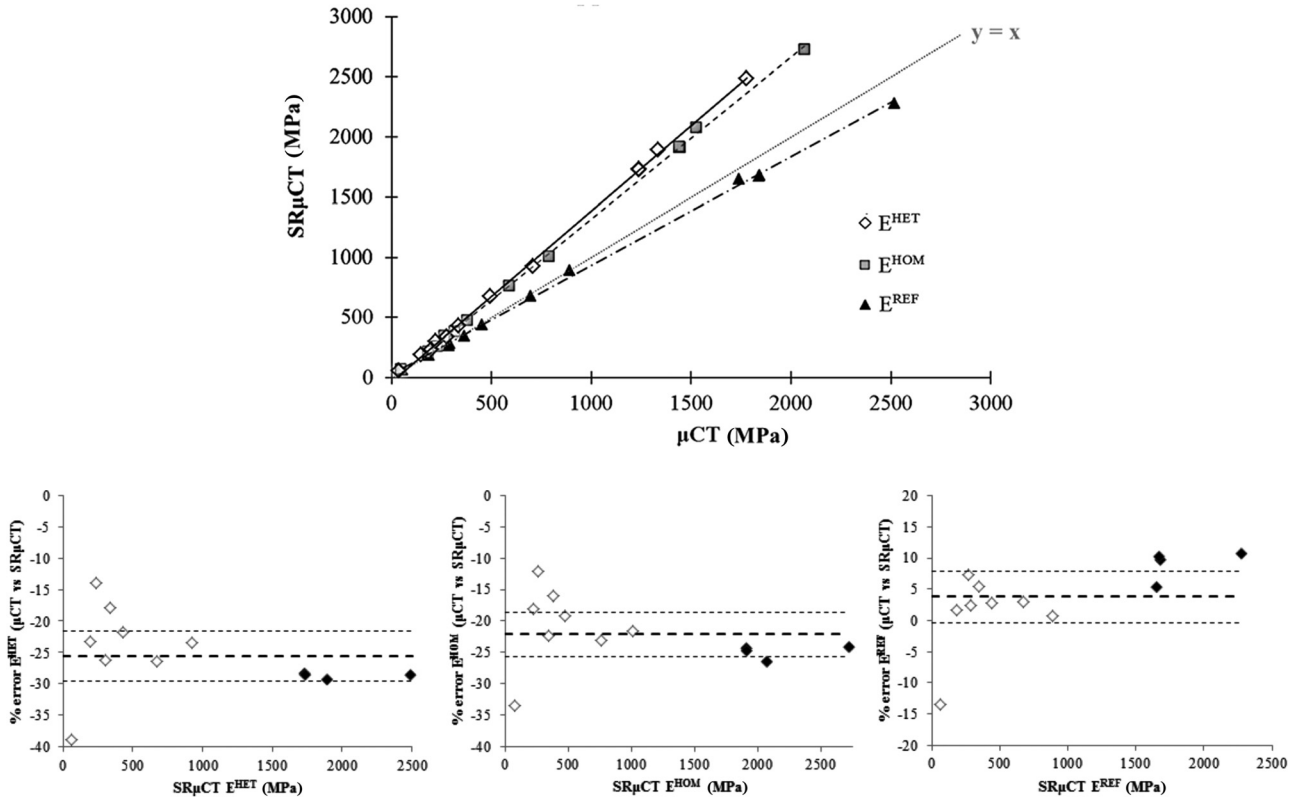

Fig. 3 Regressions and Bland–Altman analyses of E^{HET}, E^{HOM}, and E^{REF} demonstrate that the μCT-based FE analysis underestimates apparent modulus when models are specimen-specific. Regression results follow: E^{HET} $y = 1.42x - 32$ $R^2 = 0.99$; E^{HOM} $y = 1.34x - 27$ $R^2 = 0.99$; E^{REF} $y = 0.90x + 28$ $R^2 = 0.99$. In the Bland–Altman plots, empty and filled markers represent low and high BV/TV samples, respectively.

MPa) and 12% (0.12 MPa/MPa) for μCT and SRμCT models, respectively (each $p < 0.0005$).

The effect of including intraspecimen TMD heterogeneity was greater for μCT models than for SRμCT models and caused μCT models to underestimate apparent modulus. To isolate the influence of intraspecimen TMD variations, we evaluated the normalization E^{HET}/E^{HOM}. Any microstructure effects are eliminated, as well as effects related to the mean mineralization of the specific specimen. Hence, this normalization depicts solely the effect of intraspecimen mineral distribution. Again, normalization with E^{HOM} eliminated the distinction between low and high BV/TV groups; therefore, all specimens were considered together. Bland–Altman analysis revealed a 5% underestimation of E^{HET}/E^{HOM} values for μCT data compared to SRμCT data (Fig. 6).

Discussion

This study confirms that incorporating TMD spatial variation into FE models of human trabecular bone reduces the calculated apparent stiffness compared to homogeneous TMD models. We

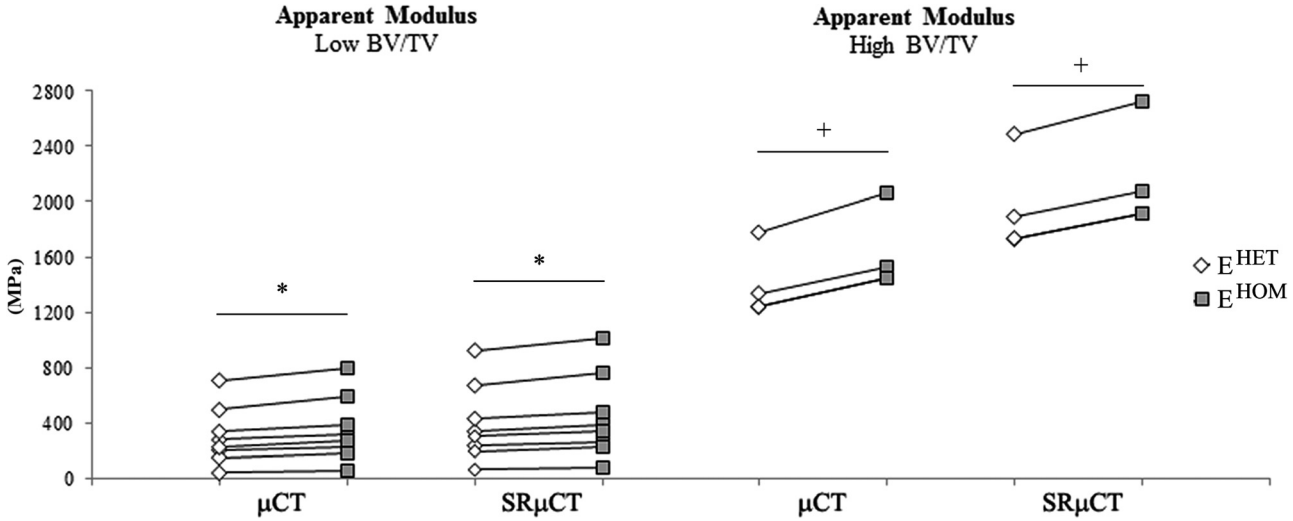

Fig. 4 Apparent modulus for the μCT and SRμCT images, stratified by low ($n = 8$) versus high ($n = 4$) BV/TV. *$p = 0.008$, + $p = 0.125$. Combined analysis (low and high BV/TV groups together) results in $p = 0.0005$.

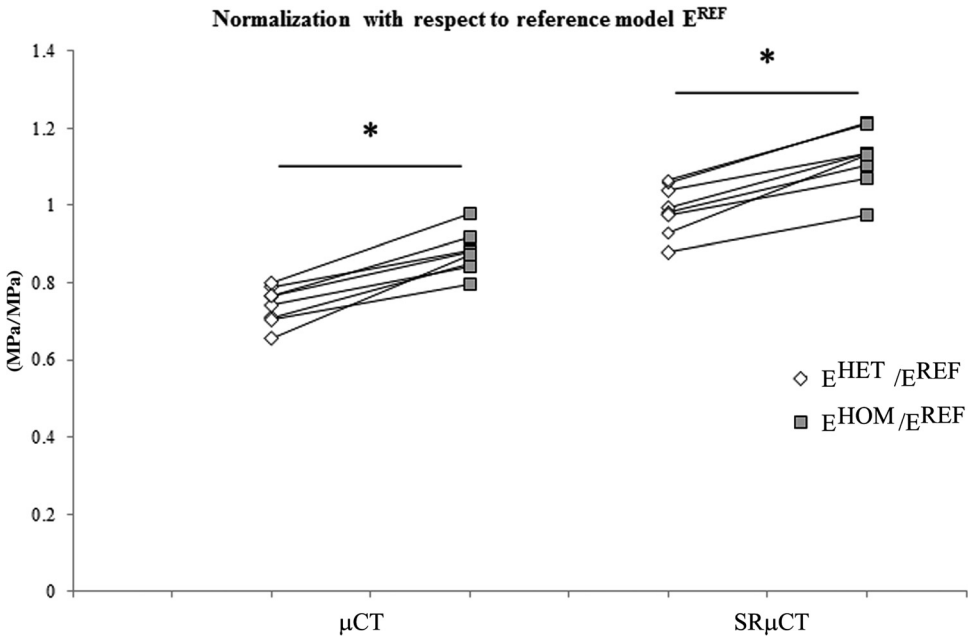

Fig. 5 Normalized apparent modulus of the μCT and SRμCT images. *$p = 0.0005$

show that this effect exists for both μCT- and SRμCT-based FE models and for trabecular bone from different anatomic sites. These results are consistent with the previous work reporting that incorporation of spatial mineral heterogeneities in μCT-based computational models leads to a reduction in apparent stiffness [11,14–16,19]. In the single previous study to investigate this effect in SRμCT-based models, Gross et al. also found that the incorporation of spatial mineral heterogeneity leads to a reduction in apparent stiffness [31]. Our study provides a direct comparison of μCT-based FE models to gold standard SRμCT-based FE models. We are thereby able to conclude that including TMD heterogeneity in μCT-based models overestimates the influence of TMD variation.

Including intraspecimen TMD heterogeneity in μCT-based FE models overestimates the influence of TMD variation. The μCT images produced larger discrepancies between the homogeneous and the heterogeneous TMD models. These results follow directly from differences in the distribution of grayscales and consequently TMD detected by μCT and SRμCT; μCT scans detected lower mean TMD values but higher intraspecimen TMD variance than SRμCT scans. Compared to SRμCT scanning, conventional polychromatic μCT scanning produces relatively lower contrast and signal-to-noise and is subject to beam-hardening [20,32–35], all of which may contribute to this outcome.

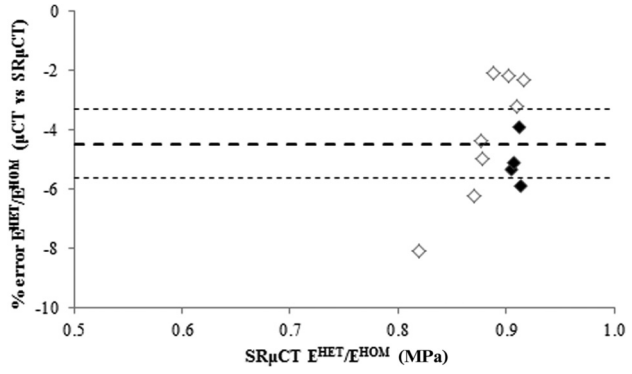

Fig. 6 Bland-Altman plot comparing μCT to SRμCT results for the normalized apparent modulus E^{HET}/E^{HOM}. Dark dashed line is the mean, light dashed lines are the 95% CI. Empty and filled markers represent low and high BV/TV samples, respectively.

A well-known limitation of conventional polychromatic μCT imaging is that TMD quantification is confounded by beam-hardening artifacts. Despite the use of beam-hardening correction algorithms, μCT-measured mean TMD underestimates SRμCT-measured mean TMD and ash densities [20]. In fully mineralized bone, beam-hardening artifacts can reduce the measured mean TMD by up to 20% [33]. The trend of TMD underestimation by μCT was observed in this present study and resulted in apparent modulus underestimation in the μCT-based models.

High-resolution FE studies of human and animal bone typically use μCT-based models with homogeneous TMD [2–4]. Though the previous studies have concluded that both μCT artifacts and the assumption of homogeneous TMD distribution would have little impact on studies that make relative comparisons of FE outcomes [19,31], these factors may have a more important effect on studies in which absolute magnitudes of the FE predictions are important. In particular, effective properties of bone tissue that are determined by calibrating FE predictions with experiments will be influenced by these errors. Therefore, μCT-based homogeneous models are suitable to study and determine overall trends and mechanisms, but in establishing absolute properties SRμCT-based heterogeneous models are theoretically more accurate.

High correlations ($R^2 > 0.99$) were found between apparent moduli calculated from μCT- and SRμCT-based FE models. This implies that post hoc scaling may be used to correct results of μCT-based models. This may be a more feasible alternative to SRμCT imaging for studies aiming to quantifying absolute biomechanical properties.

This study has some limitations. First, it is possible that differences in apparent stiffness calculated from the μCT and SRμCT reconstructions could be influenced by misalignment of the specimens between scans. However, these cylindrical specimens were machined with flat, parallel faces using a precision rotary saw blade in an effort to minimize any potential misalignment. Second, the results found here may not be applicable to μCT and SRμCT scanning at different resolutions. The voxel size of the μCT and SRμCT scans used in this study was 8 μm. It is possible that greater differences may be found between μCT and SRμCT scans at lower resolutions due to greater volume averaging effects and less accurate microstructure data. Hence, the influence of

including TMD heterogeneity may be related to the scanning resolution. Finally, the biomechanical measures examined here represent one aspect of structural integrity. These results may not capture completely the effects of TMD heterogeneity on—for example—fracture mechanics of trabecular bone.

In conclusion, we have found that including TMD heterogeneity in μCT-based FE models results in underestimation of apparent modulus. In addition, μCT imaging artifacts underestimate TMD, resulting in additional underestimation of apparent modulus in μCT-based FE models. These errors compound, with the result that a heterogeneous μCT-based model underestimates apparent modulus by 26%. Therefore, our data lead us to recommend that μCT-based FE models either (1) include TMD heterogeneity and employ a post hoc scaling correction or (2) absent an appropriate correction set, do not include TMD heterogeneity.

Acknowledgment

The authors would like to thank Steve Jorgensen, John Dunsmuir, and Andrew Burghardt for their assistance in the acquisition of synchrotron data. Funding for this research was provided by NIH F32 AR053446 (G.J.K.) and K01 AR056734 (G.J.K.). N.K. was supported by Fulbright and Noram scholarships. Scan time provided by the Brookhaven National Laboratory National Synchrotron Light Source. Computational resources were provided through the National Science Foundation via XSEDE, Grant No. TG-MCA00N019 (T.M.K.).

References

[1] Bevill, G., Eswaran, S. K., Farahmand, F., and Keaveny, T. M., 2009, "The Influence of Boundary Conditions and Loading Mode on High-Resolution Finite Element-Computed Trabecular Tissue Properties," Bone, **44**(4), pp. 573–578.

[2] Kabel, J., van Rietbergen, B., Dalstra, M., Odgaard, A., and Huiskes, R., 1999, "The Role of an Effective Isotropic Tissue Modulus in the Elastic Properties of Cancellous Bone," J. Biomech., **32**(7) pp. 673–680.

[3] Ladd, A. J., Kinney, J. H., Haupt, D. L., and Goldstein, S. A., 1998, "Finite-Element Modeling of Trabecular Bone: Comparison With Mechanical Testing and Determination of Tissue Modulus," J. Orthop. Res., **16**(5), pp. 622–8.

[4] Ulrich, D., Hildebrand, T., Van Rietbergen, B., Müller, R., and Rüegsegger, P., 1997, "The Quality of Trabecular Bone Evaluated With Micro-Computed Tomography, FEA, and Mechanical Testing," Stud. Health Technol. Inf., **40**, pp. 97–112.

[5] Van Rietbergen, B., Weinans, H., Huiskes, R., and Odgaard, A. A., 1995, "New Method to Determine Trabecular Bone Elastic Properties and Loading Using Micromechanical Finite Element Models," J. Biomech., **28**(1), pp. 69–81.

[6] Boivin, G., and Meunier, P. J., 2002, "Changes in Bone Remodeling Rate Influence the Degree of Mineralization of Bone," Connect. Tissue Res., **43**(2–3), pp. 535–537.

[7] Paschalis, E. P., Betts, F., DiCarlo, E., Mendelsohn, R., and Boskey, A. L., 1997, "FTIR Microspectroscopic Analysis of Normal Human Cortical and Trabecular Bone," Calcif. Tissue Int., **61**(6), pp. 480–486.

[8] Misof, B. M., Roschger, P., Cosman, F., Kurland, E. S., Tesch, W., Messmer, P., Dempster, D. W., Nieves, J., Shane, E., Fratzl, P., Klaushofer, K., Bilezikian, J., and Lindsay, R., 2003, "Effects of Intermittent Parathyroid Hormone Administration on Bone Mineralization Density in Iliac Crest Biopsies From Patients With Osteoporosis: A Paired Study Before and After Treatment," J. Clin. Endocrinol. Metab., **88**(3), pp. 1150–1156.

[9] Roschger, P., Rinnerthaler, S., Yates, J., Rodan, G. A., Fratzl, P., and Klaushofer, K., 2001, "Alendronate Increases Degree and Uniformity of Mineralization in Cancellous Bone and Decreases the Porosity in Cortical Bone of Osteoporotic Women," Bone, **29**(2), pp. 185–191.

[10] Yao, W., Cheng, Z., Koester, K. J., Ager, J. W., Balooch, M., Pham, A., Chefo, S., Busse, C., Ritchie, R. O., and Lane, N. E., 2007, "The Degree of Bone Mineralization is Maintained With Single Intravenous Bisphosphonates in Aged Estrogen-Deficient Rats and Is a Strong Predictor of Bone Strength," Bone, **41**(5), pp. 804–812.

[11] Bourne, B. C., and van der Meulen, M. C., 2004, "Finite Element Models Predict Cancellous Apparent Modulus When Tissue Modulus Is Scaled From Specimen CT-Attenuation," J. Biomech., **37**(5), pp. 613–621.

[12] Bouxsein, M. L., 2003, "Bone Quality: Where Do We Go From Here?," Osteoporosis Int., **14**(5), pp. S118–S127.

[13] Burr, D. B., 2004, "Bone Quality: Understanding What Matters," J. Musculoskeletal Neuronal Interact., **4**(2), pp. 184–186.

[14] Jaasma, M. J., Bayraktar, H. H., Niebur, G. L., and Keaveny, T. M., 2002, "Biomechanical Effects of Intraspecimen Variations in Tissue Modulus for Trabecular Bone," J. Biomech., **35**(2), pp. 237–246.

[15] Mulder, L., van Ruijven, L. J., Koolstra, J. H., and van Eijden, T. M., 2007, "Biomechanical Consequences of Developmental Changes in Trabecular Architecture and Mineralization of the Pig Mandibular Condyle," J. Biomech., **40**(7), pp. 1575–1582.

[16] Renders, G. A., Mulder, L., Langenbach, G. E., van Ruijven, L. J., and van Eijden, T. M., 2008, "Biomechanical Effect of Mineral Heterogeneity in Trabecular Bone," J. Biomech., **41**(13), pp. 2793–2798.

[17] van der Linden, J. C., Birkenhager-Frenkel, D. H., Verhaar, J. A., and Weinans, H., 2001, "Trabecular Bone's Mechanical Properties Are Affected by Its Non-Uniform Mineral Distribution," J. Biomech., **34**(12), pp. 1573–1580.

[18] Jaasma, M. J., Bayraktar, H. H., Niebur, G. L., and Keaveny, T. M., 2001, "The Effects of Intraspecimen Variations in Tissue Modulus on the Apparent Mechanical Properties of Trabecular Bone," Transactions of the Annual Meeting—Orthopaedic Research Society, San Francisco, p. 513.

[19] Easley, S. K., Jekir, M. G., Burghardt, A. J., Li, M., and Keaveny, T. M., 2010, "Contribution of the Intra-Specimen Variations in Tissue Mineralization to PTH and Raloxifene-Induced Changes in Stiffness of Rat Vertebrae," Bone, **46**(4), pp. 1162–1169.

[20] Kazakia, G. J., Burghardt, A. J., Cheung, S., and Majumdar, S., 2008, "Assessment of Bone Tissue Mineralization by Conventional X-Ray Microcomputed Tomography: Comparison With Synchrotron Radiation Microcomputed Tomography and Ash Measurements," Med. Phys., **35**(5), pp. 3170–3179.

[21] Feldkamp, L. A., Goldstein, S. A., Parfitt, A. M., Jesion, G., and Kleerekoper, M., 1989, "The Direct Examination of Three-Dimensional Bone Architecture in vitro by Computed Tomography," J. Bone Miner. Res., **4**(1), pp. 3–11.

[22] Burghardt, A. J., Kazakia, G. J., Laib, A., and Majumdar, S., 2008, "Quantitative Assessment of Bone Tissue Mineralization With Polychromatic Micro-Computed Tomography," Calcif. Tissue Int., **83**(2), pp. 129–138.

[23] Jorgensen, S. M., Demirkaya, O., and Ritman, E. L., 1998, "Three-Dimensional Imaging of Vasculature and Parenchyma in Intact Rodent Organs With X-Ray Micro-CT," Am. J. Physiol., **275**(3), pp. H1103–H1114.

[24] Ding, M., Odgaard, A., and Hvid, I., 1999, "Accuracy of Cancellous Bone Volume Fraction Measured by Micro-CT Scanning," J. Biomech., **32**(3), pp. 323–326.

[25] Goodenough, D., Weaver, K., Davis, D., and LaFalce, S., 1982, "Volume Averaging Limitations of Computed Tomography," Am. J. Roentgenol., **138**(2), pp. 313–316.

[26] Adams, M. F., Bayraktar, H. H., Keaveny, T. M,, and Papadopoulos, P., 2004, "Ultrascalable Implicit Finite Element Analyses in Solid Mechanics With Over a Half a Billion Degrees of Freedom," Proceeding of the ACM/IEEE High Performance Networking and Computing, Nov. 6–12, p. 34.

[27] Bevill, G., and Keaveny, T. M., 2009, "Trabecular Bone Strength Predictions Using Finite Element Analysis of Micro-Scale Images at Limited Spatial Resolution," Bone, **44**(4), pp. 579–584.

[28] Currey, J. D., 1988, "The Effect of Porosity and Mineral Content on the Young's Modulus of Elasticity of Compact Bone," J. Biomech., **21**(2), pp. 131–139.

[29] Schaffler, M. B., and Burr, D. B., 1988, "Stiffness of Compact Bone: Effects of Porosity and Density," J. Biomech., **21**(1), pp. 13–16.

[30] Kaneko, T. S., Pejcic, M. R., Tehranzadeh, J., and Keyak, J. H., 2003, "Relationships Between Material Properties and CT Scan Data of Cortical Bone With and Without Metastatic Lesions," Med. Eng. Phys., **25**(6), pp. 445–454.

[31] Gross, T., Pahr, D. H., Peyrin, F., and Zysset, P. K., 2012, "Mineral Heterogeneity Has a Minor Influence on the Apparent Elastic Properties of Human Cancellous Bone: A SRmuCT-Based Finite Element Study," Comput. Methods Biomech. Biomed. Eng., **15**(11), pp. 1137–1144.

[32] Fajardo, R. J., Cory, E., Patel, N. D., Nazarian, A., Laib, A., Manoharan, R. K., Schmitz, J. E., Desilva, J. M., Maclatchy, L. M., Snyder, B. D,, and Bouxsein, M. L., 2008, "Specimen Size and Porosity Can Introduce Error Into μCT-Based Tissue Mineral Density Measurements," Bone, **44**(1), pp. 176–184.

[33] Mulder, L., Koolstra, J. H., and Van Eijden, T. M., "Accuracy of Microct in the Quantitative Determination of the Degree and Distribution of Mineralization in Developing Bone," Acta Radiol., **45**(7), pp. 769–777.

[34] Nazarian, A., Snyder, B. D., Zurakowski, D., and Muller, R., 2008, "Quantitative Micro-Computed Tomography: A Non-Invasive Method to Assess Equivalent Bone Mineral Density," Bone, **43**(2), pp. 302–311.

[35] Nuzzo, S., Peyrin, F., Cloetens, P., Baruchel, J., and Boivin, G., 2002, "Quantification of the Degree of Mineralization of Bone in Three Dimensions Using Synchrotron Radiation Microtomography," Med. Phys., **29**(11), pp. 2672–2681.